Original Article

Multi-Energy Computed Tomography Breast Imaging with Monte Carlo Simulations: Contrast-to-Noise-Based Image Weighting

Déte Van Eeden, Freek C. P. Du Plessis

Department of Medical Physics, University of the Free State, Bloemfontein, South Africa

Abstract

Context: Photon-counting detectors and breast computed tomography imaging have been an active area of research. With these detectors, photons are assigned an equal weight and weighting schemes can be enabled. More weight can be assigned to lower energies, resulting in an increase in the contrast-to-noise ratio (CNR). **Aims:** The aim of this study is to develop and evaluate an energy weighting imaging technique to improve the CNR of simulated breast phantoms and to improve tumour detection. **Materials and Methods:** Breast phantoms consisting of adipose, glandular, malignant tissues and iodine contrast were constructed with BreastSimulator software. The phantoms were used in egs_cbct simulations for energies ranging between 20 and 65 keV from which multiple images were reconstructed. A new CNR-based image weighting method was proposed based on the CNR values obtained from the images. This method improves on previous methods and can be applied to complicated phantoms since no structural information is needed. **Results:** An increase in the CNR can be seen for lower energies. A sharp increase in the CNR is seen just above the K-edge for the phantoms with the iodine contrast. The CNR-based image weighting leads to a 68.47% (1.68-fold) increase in the CNR for the malignant tissue without iodine. For the malignant tissue with iodine contrast, the increase in the CNR was 96.14% (1.96-fold). **Conclusions:** The new proposed CNR-based image weighting scheme is easy to implement and can be used for complicated phantoms with varying structures. A large increase in the CNR is seen with or without the use of iodine contrast.

Keywords: Image weighting, Monte Carlo, multi-energy computed tomography

Received on: 02-05-2018 **Review completed on: 17-04-2019** **Accepted on: 17-04-2019**

Introduction

Conventional mammography is often used for the early detection of cancer, despite its limitations of tissue overlapping in dense breasts.[1-4] The sensitivity for this technique is about 85% and it reduces to 47.8-64.4% for dense breasts.[5] Breast computed tomography (CT) has been an active area of research with promising outcomes that can reduce the structural overlap of mammography.[6-10] Boone *et al*.[11] showed that the dose received from breast CT was comparable to that for two-view mammography for 5-cm thickness compressed breasts. Breast CT systems usually consist of a cone-beam geometry and flat panel detectors.

Due to the recent advances in detector technology, these integrating flat panel detectors can now be replaced by photon-counting detectors. These detectors are capable of counting discrete photon interactions, and multiple monoenergetic images can be obtained with single image acquisition. Several studies have been conducted with multi-energy CT[12-14] and include K-edge imaging using contrast agents.[9,15] These contrast images can be used for tissue differentiation or quantification and proved to be useful in multiple studies.[16-18] There occurs a sharp increase in the contrast between the iodinated malignant and glandular tissue slightly above the absorption edge of iodine.

Conventional integrating detectors weigh each photon by its energy, and therefore, more weight is given to the higher energies. The contribution of lower energies is less and substandard contrast is achieved since the contrast between materials is the best at lower energies. Photon-counting detectors assign equal weight to all the photons, and optimal weighting schemes can be developed to maximize the contrast-to-noise ratio (CNR).

Access this article online

Quick Response Code:

Website: www.jmp.org.in

DOI: 10.4103/jmp.JMP_48_18

Address for correspondence: Dr. Déte Van Eeden, Department of Medical Physics, University of the Free State, P.O. Box 339, Bloemfontein 9300, South Africa.
E-mail: VaneedenD@ufs.ac.za

How to cite this article: Van Eeden D, Du Plessis FC. Multi-energy computed tomography breast imaging with Monte Carlo simulations: Contrast-to-noise-based image weighting. J Med Phys 2019;44:106-12.

Breast tumour contrast is higher at lower energies due to linear attenuation coefficient properties of breast tissue.[19] Higher energies will lead to a decrease in the contrast between glandular breast tissue and malignant tissue. However, using a low kV setting for image acquisition will not be feasible since it will lead to an increase in image noise. Energy spectrums usually consist of a small fraction of low-energy photons that is insufficient for image acquisition and will lead to high statistical variances. Therefore, additional information from higher energies with more photons and better statistics is needed for adequate images.

Energy weighting can be used to weigh the different energies to obtain an image with the best contrast possible. X-ray beam energy intervals are divided into several bins, depending on the capabilities of the photon-counting detector. These weighting schemes entail giving different energy bins different weights producing a combined image with a maximum CNR.

CNR improvement with X-ray weighting was first proposed in 1985 by Tapiovaara and Wagner.[20] Further studies included a simulation study by Giersch *et al*.,[21] and the practical feasibility was investigated by Niederlöhner *et al*.[22] Shikhaliev[23,24] conducted several studies that included the effect of energy weighting on beam hardening and the use of a tilted angle cadmium zinc telluride detector. In 2008, he found an increase in the CNR for breast tissues of 1.16–1.36 when using energy weighting CT.[10] These results show that weighted energy-resolved data are a further improvement on photon-counting detectors and aid in constructing an image with the highest CNR achievable.[25]

The projection data of each energy bin can be weighted before image reconstruction, or each reconstructed image can be weighted and then combined to form a final image. Niederlöhner *et al*.[26] first proposed an image-based energy weighting scheme and found a reduction in the cupping effect by applying the weighting after reconstruction and also an increase in the image quality. The Downhill-Simplex method is applied after the first step of the reconstruction process and uses a trial algorithm to find the optimum weighting function.[27]

Schmidt[28] used an analytical method to determine the weights that will yield an image with a maximum CNR. Their study included a projection-based and image-based energy weighting scheme. The length of the contrast material is used during the projection-based energy weighting, and the image-based energy weighting uses the reconstructed attenuation coefficients of the image. These parameters are easy to obtain when using a simple phantom with known inserts. However, it is not always feasible when phantoms are based on clinical data with varying structures. The length and shape of each structure can vary for the different projections, making it difficult to obtain specific parameter information. Depending on the reconstruction algorithm used and the processing of the images, the pixel values in the images may not represent the attenuation coefficients at all. In another study by Le Huy *et al*.,[29] a spectral model and the effective attenuation coefficients were used for the determination of the weighting factors. Both these studies are limited to phantom studies with simple geometries but are difficult to apply to other more complex geometries, such as the breast phantoms found in this study.

In this study, image-based energy weighting was explored with weights based on the CNRs of the different energy bin images. No structural information is needed before using this weighting method, making it more suitable for complex cases. This method is an improvement on previous studies and is easier to implement.

Materials and Methods

Breast phantom modeling

The BreastSimulator software package by Bliznakova *et al*.[30,31] was used to model a breast phantom. The phantom consisted of ducts and Cooper's ligaments that formed the glandular tissue. Malignant tissue was embedded in the glandular tissue, and the rest of the breast consisted out of adipose tissue. One of the malignant tumours contained 8 mg/mL iodine that is frequently used as a contrast agent to improve the contrast during imaging with a K-edge peak at 33.2 keV. The elemental composition of all the tissues was obtained from the International Commission on Radiation Units and Measurements report 44, and the malignant tissue was assumed to be equivalent to pork muscle, as reported by previous studies.[32-35]

Monte Carlo simulations and image reconstruction

The egs_cbct code was used for the simulation of the breast phantom. It is an EGSnrc[36] user code written in C++ by Mainegra-Hing and Kawrakow[37,38] and was released in March 2013 with EGSnrc V4 2.4.0. The egs_cbct code can simulate a complete cone-beam CT (CBCT) imaging system and is mainly used for the fast estimation of the scatter contribution as seen in previous studies.[39-42] It has also recently been used in the simulation of a fan-beam geometry.[43] Several variance reduction techniques together with a denoising algorithm are used by this code to improve scatter simulation efficiency. These techniques are described in one of the original papers[37] and also in a further paper by Thing and Mainegra-Hing.[39]

A cone-beam geometry was used with a cadmium telluride (CdTe) detector. The X-ray beam energy spectrum was subdivided into 10 energies ranging between 20 and 65 keV in 5 keV increments and was used to obtain reconstructed images of the breast phantom, each obtained for a certain beam energy interval. The width of the bins was chosen to include the K-edge of the iodine contrast agent to minimize the effects of photon starvation due to the high attenuation of the iodine.[44,45] Projection images were taken over a 360° arc with 1 billion histories per projection, resulting in a statistical variance below 1%. The simulations were performed on a high-performance computer unit consisting of 1520 cores and 28 nodes. Each node consists of random access memory between 96 and 128 GB, and the network used is quad data rate with 40 GB/s throughput and low latency.

The XCOM photon cross-section compilation[46] was used during the simulations. Rayleigh scattering and Compton scattering with binding corrections were implemented. The photon cut-off energy and electron cut-off energy (ECUT) values were 0.001 and 1.000 MeV, respectively. Electron transport was avoided by choosing a very high value for ECUT.

The simulations were performed with a point source and rectangular collimation with a source-to-axis distance of 55 cm and a source-to-detector distance of 100 cm. A 28 cm × 16 cm CdTe detector was used with a density of 5.85 g/cm^3 and voxel sizes of 0.08 cm. The egs_cbct simulation geometry is shown in Figure 1.

A log transformation with a blank (air) scan is done in order to obtain a projection image as seen below.

Projection image = -log(raw detector data)÷blank scan data

The Feldkamp–Davis–Kress filtered back-projection algorithm was used for the reconstruction of the images using the Open Source Cone-beam Reconstructor (OSCaR) software from the American Association of Physicists in Medicine.[47] The software consists of a graphical user interface and a MATLAB code for image reconstruction and processing. Images were reconstructed with a 0.05 cm voxel size using a Shepp-Logan filter.

Contrast-to-noise ratio determination

The CNR for the images was obtained with the aid of an in-house developed interactive data language code. The code assigns segments to the structures through the Canny edge detection algorithm.[48] Thereafter, the region of interest (ROI) is selected for the adipose, glandular, and malignant tissues on all the images. Equation (1) was used to determine the CNR for each reconstructed image.

$$\mathrm{CNR} = \frac{|S_M - S_G|}{\sigma_B} \quad (1)$$

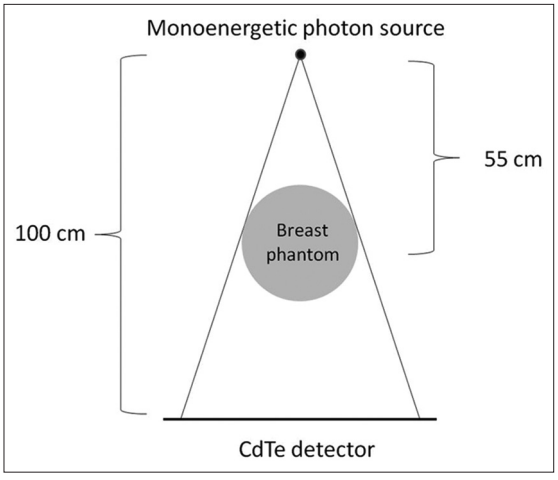

Figure 1: The egs_cbct simulation set-up of the various breast phantoms

where S_M and S_G are the signals in the malignant and glandular tissue, respectively. The background standard deviation, σ_B, is taken in the uniform adipose tissue.

Energy weighting and its application

The weighting factor w_i for each energy i was defined as its normalized CNR_i value using Equation (2).

$$w_i = \left(\frac{CNR_i}{CNR_{max}} \right) \quad (2)$$

where CNR_{max} is the highest CNR obtained. The energy with the highest CNR_i will have a weighting factor of 1.

The image-based energy weighting was done after the reconstruction of the images. A schematic of the process is presented in Figure 2. Weighting factors were used to scale the different images (and after summation) formed a final energy-weighted image. Each reconstructed image (at energy bin i) is multiplied by its weighting factor and then added together to form the final image.

The combined CNR, CNR_{tot}, is calculated as:[28]

$$CNR_{tot} = \frac{\sum_{i=1}^{t} w_i C_i}{\left(\sum_{i=1}^{t} w_i^2 \sigma_b^2 \right)^{1/2}} \quad (3)$$

where C_i is the absolute contrast between the malignant tissue and glandular tissue in each image.

The standard deviation in the background of the images is given by σ_b, and the weighting factor (calculated with Equation [2]) for each energy bin is w_i.

Results

Slices through the actual breast model obtained with the BreastSimulator software are presented in Figure 3.

These projection images were reconstructed with OSCaR employing a Shepp-Logan filter with a voxel size of 0.05 cm.

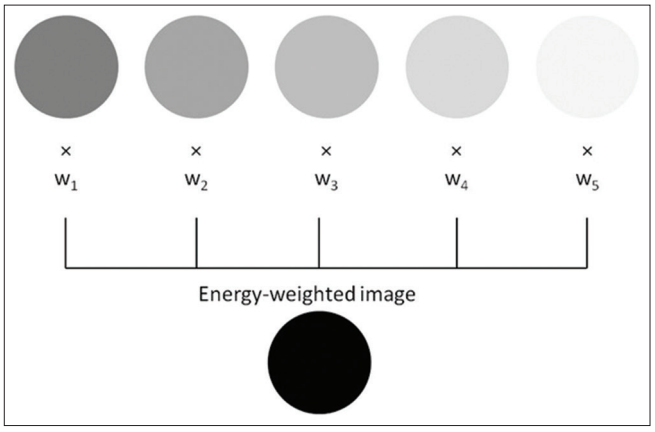

Figure 2: A schematic of the resulting image (bottom) obtained by weighing each image (top row) first and then adding them up. Here, for example, five images were used representing five energy bins

Figure 4 shows the same image slice but reconstructed at energies between 20 and 65 keV. Figure 5 shows a reconstructed breast slice at the various energies with 8 mg/mL iodine contrast agent.

The Canny edge detection algorithm[48] was used to determine the ROIs for the different images. The edge detection image was superimposed onto the reconstructed image as shown in Figure 6.

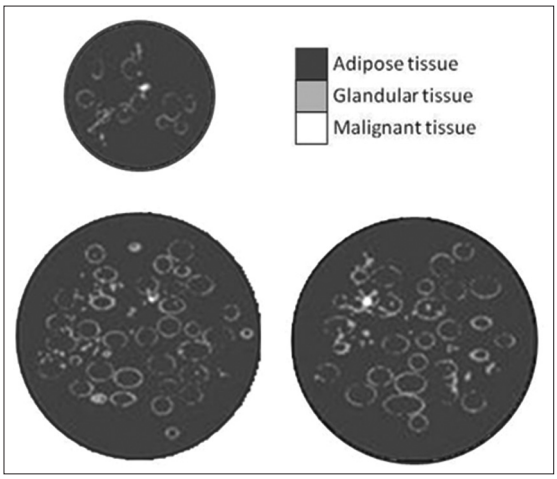

Figure 3: Slices through the breast phantom consisting out of glandular, adipose, and malignant tissue. The top image contained the 8 mg/mL iodine contrast agent

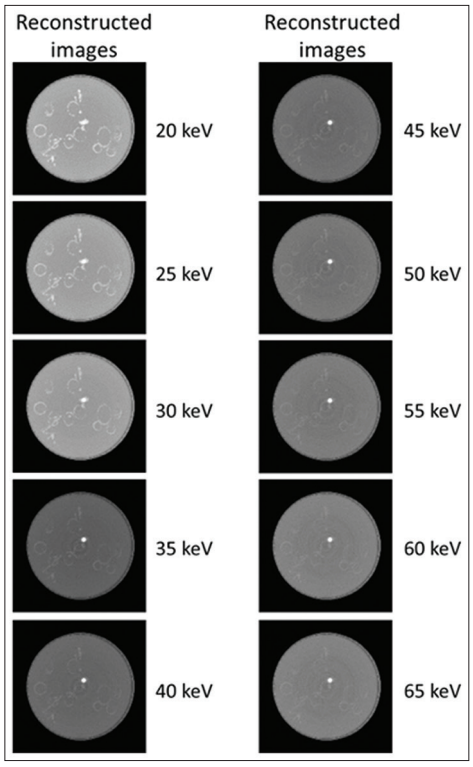

Figure 5: The reconstructed images from 20 to 65 keV. The malignant tissue contained 8 mg/mL iodine contrast agent and is seen as a white dot in the images

The CNRs were calculated for each energy with Equation (1) as shown in Figure 7.

In Figure 7, the CNR values decrease at higher energy since the probability for photoelectric events reduces at higher photon energy. Albeit, Compton scattering increases with increasing energy and depends on the relative electron density of the tumour and the background soft tissue. A sharp increase in contrast is seen when the tumour absorbs iodine, as shown in Figure 8. The effect of iodination increases the CNR value

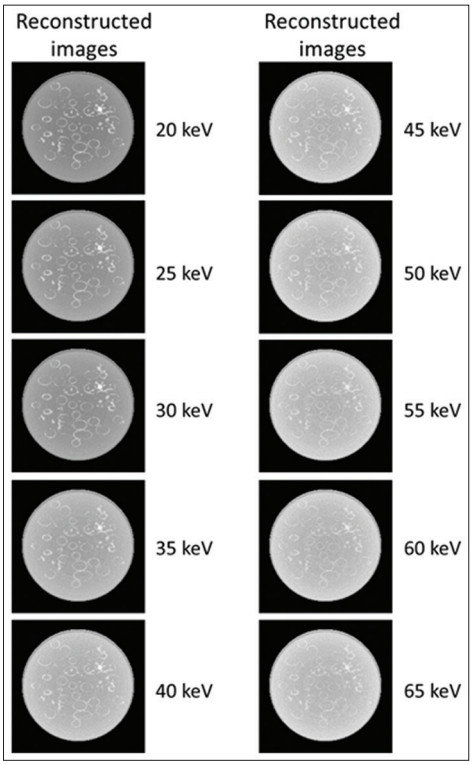

Figure 4: The reconstructed images from 20 to 65 keV of a slice through the breast phantom. The malignant tissue does not contain any iodine contrast agent

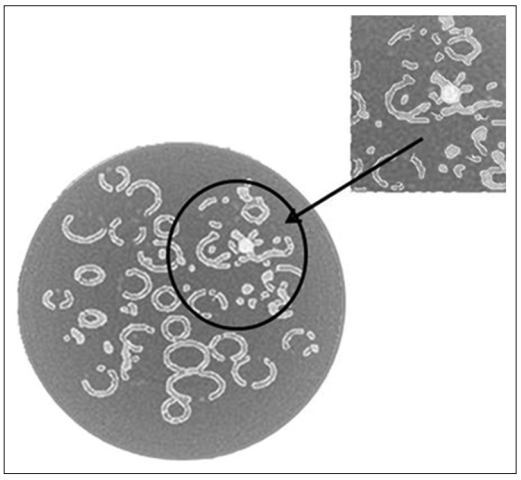

Figure 6: The Canny edge detection algorithm superimposed onto the reconstructed image to determine the regions of interest. The smaller images is a magnification of the area consisting of the malignant tissue

nearly tenfold beyond the absorption edge of 33.2 keV. The difference in the two data sets, Figures 7 and 8 suggests that low photon energy is more desirable for good CNR whereas optimal energy of 35 keV would result in the best CNR value for iodinated tumours.

From Equation (2), the weights were determined for the different energy levels.

A comparison between the highest CNR and the CNRs obtained with the weighting factors is presented in Figure 9. The highest CNR for the iodine contrast is obtained at 35 keV and for the mass without iodine at 20 keV. The CNR with the weighting factors is calculated with Equation (3) for each mass.

In Figure 10, a profile comparison can be seen for the iodinated malignant mass at the energy of 20 and 35 keV, respectively. There occurs an increase in the malignant mass signal, and the shape is also more defined as with the energy of 20 keV. The increase in the background noise for the 20 keV is also evident.

In Figure 11, a profile comparison is seen between two images obtained with different weighting methods. A CNR-weighted image was obtained using the weights calculated with Equation (3), and the profile is seen with a solid line in Figure 11. A second image was obtained representing that of a photon-counting detector with weighting factors of 1 for each energy bin.

It can be seen from Figure 11 that the difference between the malignant tissue signal and the surrounding structures increases when the weights are applied. This will result in an increase in the CNR.

In Figure 12, the increase in the CNR can be seen when the weighting is applied. For the malignant mass without any contrast, the CNR increase is 68.47% in comparison with 20 keV. For the malignant mass with the iodine contrast, the increase in the CNR is 96.14% in comparison with 35 keV.

An increase of 35.55% and 25.54% can be seen, without and with iodine contrast, respectively, when using image-based

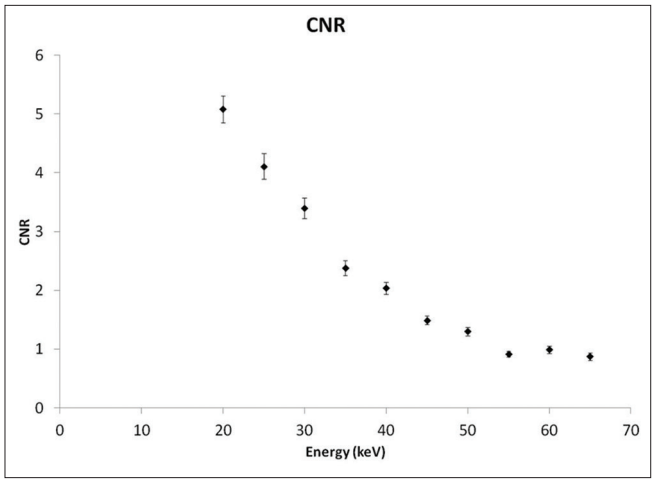

Figure 7: Calculated contrast-to-noise ratio at different energy levels for the malignant mass without iodine

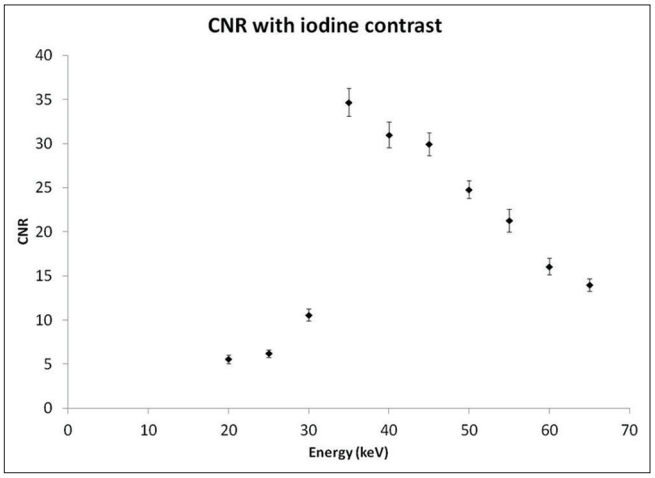

Figure 8: A sharp increase in contrast-to-noise ratio is related to iodinated malignant tissue slightly above the absorption edge of iodine

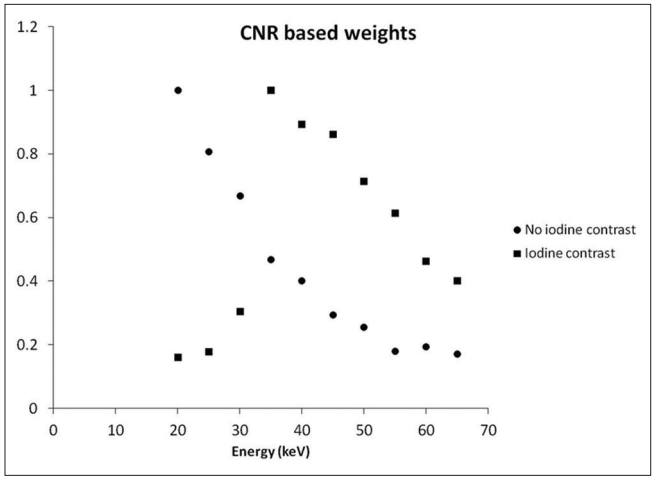

Figure 9: The weighting factors for the different energies based on the contrast-to-noise ratios seen in Figures 7 and 8

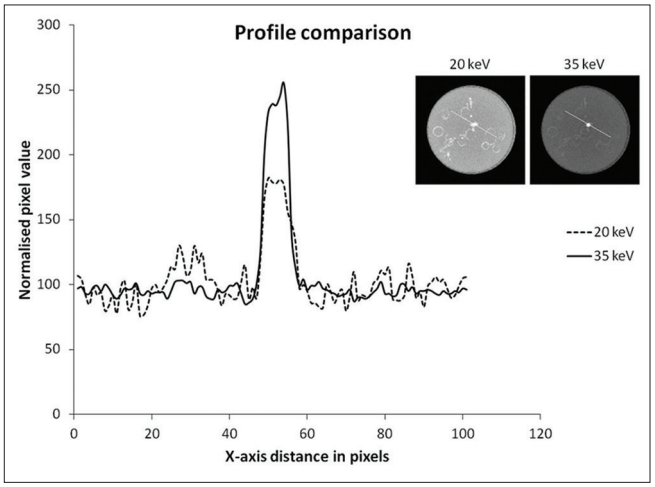

Figure 10: The profile comparison between 20 and 35 keV energy bin for the iodinated malignant mass

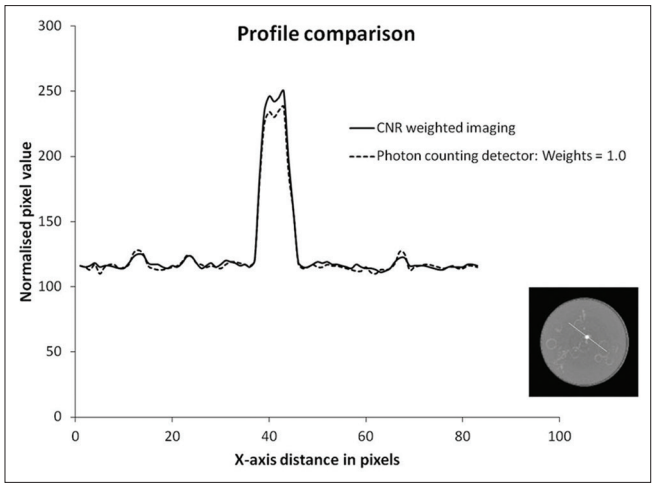

Figure 11: A profile comparison between images with contrast-to-noise ratio-based weights and an image with equal weights for each bin

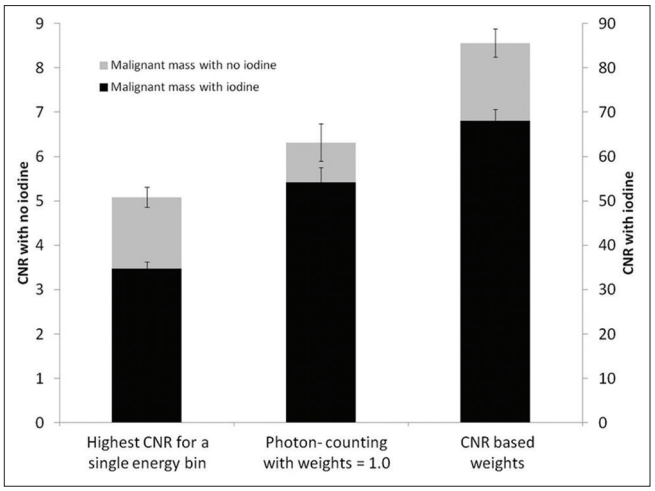

Figure 12: A comparison of the contrast-to-noise ratio obtained with a single energy bin (20 keV for malignant mass without contrast and 35 keV for the iodinated malignant mass), equal weights of 1 and weighting factors based on the contrast-to-noise ratio. Note that the contrast-to-noise ratio values are scaled so that contrast without iodine is read off on the left-hand y-axis

energy weighting instead of a photon-counting detector with equal weights.

Discussion

An alternative method for image-based energy weighting was explored using the CNR values of the different energy bins. For the CNR-based image weighting, the increase in the CNR for the malignant tissue without the iodine was 68.47% (1.68-fold), and for the malignant tissue with iodine contrast, the increase in the CNR was 96.14% (1.96-fold).

In Figures 10 and 11, profiles through the reconstructed image can be seen. In Figure 10, the effect of the iodine contrast on the signal can be seen between 20 and 35 keV. There occurs an increase in the iodine contrast signal at energy slightly above the absorption peak at 35 keV. There is also a decrease in the background noise when using 35 keV, due to the increase in the number of photons that leads to better statistics. In Figure 11, there is an increase in the difference between the malignant and glandular tissue signals when applying the energy weighting scheme with different weights. This will lead to an increase in CNR and better tumour detection.

The methods used in this study are an improvement on those of previous studies. The weights are based on the CNRs of the images and not on the structural information or linear attenuation coefficients. This method can be applied to simple phantoms and to complex phantoms based on clinical data. The method proposed in this study is not limited to breast tissue and can be applied to any image dataset if the CNRs are known.

Conclusions

It was found that the maximum CNR is found at the lower energies such as 20 keV. The CNR decreases as the energy increases. For the malignant tissue with the iodine contrast, the maximum CNR is found slightly above the K-edge at 35 keV.

The image-based energy weighting leads to an improvement in the CNR and is a valuable method to use. Previous studies showed improvements in the CNRs with factors of 1.31 and 1.16 for image-based weighting and projection-based weighting, respectively.[28] This is lower than the 1.68 and 1.96 found in this study with and without iodine contrast.

The method proved to be effective for the improvement in the CNRs of breast images acquired with a photon-counting detector without the need for structural information.

Acknowledgment

The authors thank the Medical Research Council of South Africa and Mrs. T. Mulder, Medical Editor, School of Medicine, University of the Free State, for technical and editorial preparation of the manuscript.

Financial support and sponsorship

This research project was funded by the South African Medical Research Council with funds from the National Treasury under its Economic Competitiveness and Support Package. This research and the publication thereof is the result of funding provided by the Medical Research Council of South Africa in terms of the MRC's Flagships Awards Project SAMRC-RFA-UFSP-01-2013/HARD.

Conflicts of interest

There are no conflicts of interest.

References

1. Leung JW, Margolin FR, Dee KE, Jacobs RP, Denny SR, Schrumpf JD. Performance parameters for screening and diagnostic mammography in a community practice: Are there differences between specialists and general radiologists? AJR Am J Roentgenol 2007;188:236-41.
2. Fenton JJ, Egger J, Carney PA, Cutter G, D'Orsi C, Sickles EA, *et al.* Reality check: Perceived versus actual performance of community

mammographers. AJR Am J Roentgenol 2006;187:42-6.
3. Kriege M, Brekelmans CT, Boetes C, Besnard PE, Zonderland HM, Obdeijn IM, *et al.* Efficacy of MRI and mammography for breast-cancer screening in women with a familial or genetic predisposition. N Engl J Med 2004;351:427-37.
4. Leach MO, Boggis CR, Dixon AK, Easton DF, Eeles RA, Evans DG, *et al.* Screening with magnetic resonance imaging and mammography of a UK population at high familial risk of breast cancer: A prospective multicentre cohort study (MARIBS). Lancet 2005;365:1769-78.
5. Thigpen D, Kappler A, Brem R. The Role of Ultrasound in Screening Dense Breasts—A Review of the Literature and Practical Solutions for Implementation. Diagnostics 2018;8:20.
6. Lindfors KK, Boone JM, Nelson TR, Yang K, Kwan AL, Miller DF. Dedicated breast CT: Initial clinical experience. Radiology 2008;246:725-33.
7. Glick SJ. Breast CT. Annu Rev Biomed Eng 2007;9:501-26.
8. Lai CJ, Shaw CC, Chen L, Altunbas MC, Liu X, Han T, *et al.* Visibility of microcalcification in cone beam breast CT: Effects of x-ray tube voltage and radiation dose. Med Phys 2007;34:2995-3004.
9. Schlomka JP, Roessl E, Dorscheid R, Dill S, Martens G, Istel T, *et al.* Experimental feasibility of multi-energy photon-counting K-edge imaging in pre-clinical computed tomography. Phys Med Biol 2008;53:4031-47.
10. Shikhaliev PM. Energy-resolved computed tomography: First experimental results. Phys Med Biol 2008;53:5595-613.
11. Boone JM, Nelson TR, Lindfors KK, Seibert JA. Dedicated breast CT: Radiation dose and image quality evaluation. Radiology 2001;221:657-67.
12. Masetti S, Fiaschetti M, Turco A, Roma L, Rossi PL, Mariselli M, *et al.* Development of a multi-energy CT for small animals: Characterization of the quasi-monochromatic x-ray source. IEEE Trans Nucl Sci 2009;56:29-35.
13. Yang Q, Cong W, Wang G. Superiorization-based multi-energy CT image reconstruction. Inverse Probl 2017;33. pii: 044014.
14. Yu L, Leng S, McCollough CH. Dual-source multi-energy CT with triple or quadruple X-ray beams. Proc SPIE Int Soc Opt Eng 2016;9783. pii: 978312.
15. Roessl E, Proksa R. K-edge imaging in x-ray computed tomography using multi-bin photon counting detectors. Phys Med Biol 2007;52:4679-96.
16. Uotani K, Watanabe Y, Higashi M, Nakazawa T, Kono AK, Hori Y, *et al.* Dual-energy CT head bone and hard plaque removal for quantification of calcified carotid stenosis: Utility and comparison with digital subtraction angiography. Eur Radiol 2009;19:2060-5.
17. Watanabe Y, Uotani K, Nakazawa T, Higashi M, Yamada N, Hori Y, *et al.* Dual-energy direct bone removal CT angiography for evaluation of intracranial aneurysm or stenosis: Comparison with conventional digital subtraction angiography. Eur Radiol 2009;19:1019-24.
18. Yamamoto S, McWilliams J, Arellano C, Marfori W, Cheng W, Mcnamara T, *et al.* Dual-energy CT angiography of pelvic and lower extremity arteries: Dual-energy bone subtraction versus manual bone subtraction. Clin Radiol 2009;64:1088-96.
19. Johns PC, Yaffe MJ. X-ray characterisation of normal and neoplastic breast tissues. Phys Med Biol 1987;32:675-95.
20. Tapiovaara MJ, Wagner R. SNR and DQE analysis of broad spectrum x-ray imaging. Phys Med Biol 1985;30:519-29.
21. Giersch J, Niederlöhner D, Anton G. The influence of energy weighting on x-ray imaging quality. Nucl Instrum Methods Phys Res A 2004;531:68-74.
22. Niederlöhner D, Karg J, Giersch J, Anton G. The energy weighting technique: measurements and simulations. Nucl Instrum Methods Phys Res A 2005;546:37-41.
23. Shikhaliev PM. Beam hardening artefacts in computed tomography with photon counting, charge integrating and energy weighting detectors: A simulation study. Phys Med Biol 2005;50:5813-27.
24. Shikhaliev PM. Tilted angle CZT detector for photon counting/energy weighting x-ray and CT imaging. Phys Med Biol 2006;51:4267-87.
25. Rupcich F, Gilat-Schmidt T. Experimental study of optimal energy weighting in energy-resolved CT using a CZT detector. Proc SPIE 8668, Medical Imaging 2013: Physics of Medical Imaging, 86681X; 6 March, 2013.
26. Niederlöhner D, Karg J, Giersch J, Firsching M, Anton G. Practical aspects of energy weighting in x-ray imaging. IEEE Nucl Sci Symp Conf Rec 2004;5:3191-4.
27. Niederlöhner D, Nachtrab F, Michel T, Anton G. Using the Medipix2 detector for photon counting computed tomography. IEEE Nucl Sci Symp Conf Rec 2005;4:2327-31.
28. Schmidt TG. Optimal "image-based" weighting for energy-resolved CT. Med Phys 2009;36:3018-27.
29. Le Huy Q, Ducote JL, Molloi S. Radiation dose reduction using a CdZnTe-based computed tomography system: Comparison to flat-panel detectors. Med Phys 2010;37:1225-36.
30. Bliznakova K, Suryanarayanan S, Karellas A, Pallikarakis N. Evaluation of an improved algorithm for producing realistic 3D breast software phantoms: Application for mammography. Med Phys 2010;37:5604-17.
31. Bliznakova K, Sechopoulos I, Buliev I, Pallikarakis N. Breast simulator: A software platform for breast x-ray imaging research. J Biomed Graph Comput 2012;2:1.
32. Bohndiek SE, Cook EJ, Arvanitis CD, Olivo A, Royle GJ, Clark AT, *et al.* A CMOS active pixel sensor system for laboratory-based x-ray diffraction studies of biological tissue. Phys Med Biol 2008;53:655-72.
33. Elshemey WM, Elsharkawy WB. Monte Carlo simulation of x-ray scattering for quantitative characterization of breast cancer. Phys Med Biol 2009;54:3773-84.
34. Peplow DE, Verghese K. Measured molecular coherent scattering form factors of animal tissues, plastics and human breast tissue. Phys Med Biol 1998;43:2431-52.
35. Griffiths JA, Royle GJ, Hanby AM, Horrocks JA, Bohndiek SE, Speller RD. Correlation of energy dispersive diffraction signatures and microCT of small breast tissue samples with pathological analysis. Phys Med Biol 2007;52:6151-64.
36. Kawrakov I, Mainegra-Hing E, Rogers DW. The EGSnrc Code System: Monte Carlo Simulation of Electron and Photon Transport; 2010.
37. Mainegra-Hing E, Kawrakow I. Variance reduction techniques for fast Monte Carlo CBCT scatter correction calculations. Phys Med Biol 2010;55:4495-507.
38. Mainegra-Hing E, Kawrakow I. Fast Monte Carlo calculation of scatter corrections for CBCT images. Phys Conf Ser 2008;102:012017.
39. Thing RS, Mainegra-Hing E. Optimizing cone beam CT scatter estimation in egs_cbct for a clinical and virtual chest phantom. Med Phys 2014;41:071902.
40. Chang J, Zhou L, Wang S, Clifford Chao KS. Panoramic cone beam computed tomography. Med Phys 2012;39:2930-46.
41. Watson P, Mainegra-Hing E, Soisson E, Naqa IE, Seuntjens J. SU-E-I-04: Implementation of a fast Monte Carlo scatter correction for cone- beam computed tomography. Med Phys 2012;39:3625.
42. Thing RS, Bernchou U, Mainegra-Hing E, Brink C. Patient-specific scatter correction in clinical cone beam computed tomography imaging made possible by the combination of Monte Carlo simulations and a ray tracing algorithm. Acta Oncol 2013;52:1477-83.
43. van Eeden D, du Plessis F. EGS_cbct: Simulation of a fan beam CT and RMI phantom for measured HU verification. Phys Med 2016;32:1375-80.
44. Nasirudin RA, Mei K, Penchev P, Fehringer A, Pfeiffer F, Rummeny EJ, *et al.* Reduction of metal artifact in single photon-counting computed tomography by spectral-driven iterative reconstruction technique. PLoS One 2015;10:e0124831.
45. Ghadiri H, Ay MR, Shiran MB, Soltanian-Zadeh H, Zaidi H. K-edge ratio method for identification of multiple nanoparticulate contrast agents by spectral CT imaging. Br J Radiol 2013;86:20130308.
46. Berger MJ, Hubbell JH. XCOM: Photon cross sections on a personal computer [Internet]. 1987. Report No.: NBSIR-87-3597, 6016002. Available from: http://www.osti.gov/servlets/purl/6016002-Jgm0Fa/. [Last cited on 2016 Aug 02].
47. Rezvani N, Aruliah D, Jackson K, Moseley D, Siewerdsen J. SU-FF-O-16: OSCaR: an open-source cone-beam CT reconstruction tool for imaging research. Med Phys 2007;34:2341.
48. Canny Edge Detection – OpenCV-Python Tutorials 1 Documentation. Available from: http://opencv-pythontutroals.readthedocs.io/en/latest/py_tutorials/py_imgproc/py_canny/py_canny.html. [Last accessed on 2018 Apr 23].